BOLETÍN GEOLÓGICO Y MINERO 136 (1)
enero-marzo 2025, 006
ISSN-L: 0366-0176, eISSN: 2253-6167
https://doi.org/10.21701/bolgeomin/136.1/006

Boletín Geológico y Minero

RESEARCH ARTICLE

Preliminary U-Pb Zircon Geochronology of the Eburnean Menongue Igneous Complex, Cassinga Zone, Angolan Shield

Geocronología U-Pb preliminar del Complejo Ígneo de Menongue (Eburneano), Zona de Cassinga, Escudo de Angola

Ezequiel Ferreira[1,2*], Pablo Valverde-Vaquero[1], Miguel Gutíerrez-Medina[2], Jorge Buzzi-Marcos[2], Rui Lopes[2], Juan Carlos Gumiel[1,2], Enrique Merino-Martínez[1], Aratz Beranoaguirre[2], María del Carmen Feria[2], Pilar Montero[3], José Manuel[4]

[1]Instituto Geológico y Minero de España, CN-IGME-CSIC, 28760, Tres Cantos, España
[2]UTE-PLANAGEO (IGME/LNEG/Impulso), Parque tecnológico de Asturias, parcela 13A, 15 33428, Asturias, España
[3]SHRIMP Ion-Microprobe Laboratory - IBERSIMS. Centro de Instrumentación Científica. Universidad de Granada, 18002, Granada, España
[4]Instituto Geológico de Angola (IGEO), Centralidade do Kilamba, Rua 311, Luanda, Angola

Corresponding author: ezequiel.geo@gmail.com (Ezequiel Ferreira)

Key point:

New U-Pb zircon data show the Menongue Igneous Complex was emplaced during the Eburnean Event between 1982.4±22.9 and 1949.3±10.2 Ma.

Emplacement of the Menongue Igneous Complex plutonic and volcanic suites was coeval.

Our data refute previous time correlations with the Matala (Cassinga Zone) and Chibia-Cainde (Central Eburnean Zone) (sub)volcanic rocks.

ABSTRACT

The Menongue Igneous Complex (MIC) consists of a set of previously undated plutonic and volcanic rocks located within the Cassinga Zone of the Angolan Shield. The complex comprises granodiorites, monzo- to syenogranites, and subordinate diorites, quartz-diorites, and leucogranites in the plutonic suite, along with andesitic to rhyolitic coherent and pyroclastic volcanic rocks in the volcanic suite. New U-Pb zircon geochronological data obtained as part of the National Geological Plan of Angola (PLANAGEO) reveal crystallization ages ranging from 1982.4±22.9 Ma to 1949.3±10.2 Ma, demonstrating that the magmatic activity responsible for the emplacement of the MIC occurred during the Paleoproterozoic Eburnean Event (ca. 2050 Ma to 1933 Ma in the Angolan Shield). Overlapping crystallization ages of a monzogranite (1968.8±6.2 Ma) and rhyolite (1963.9±2.8 Ma) support field evidence suggesting coeval emplacement of the volcanic and plutonic facies. Additionally, our data show that the magmatism of the MIC is coeval with granitoids and felsic volcanics from Conda, in the northwestern part of the Central Eburnean Zone (1978±11 Ma to 1964±9 Ma), but dismiss previously proposed correlations with felsic (sub)volcanics from Matala, in the Cassinga Zone, and from Chibia–Cainde (1814±8 Ma to 1804±7 Ma), in the southern part of the Central Eburnean Zone. Future detailed whole-rock geochemistry and zircon U-Pb and Lu-Hf studies of the Eburnean record in the Cassinga Zone will help establish the geotectonic significance of the Cassinga Zone in the evolution of the supercontinent Columbia.

Keywords: Menongue Igneous Complex; Cassinga Zone; Angolan Shield; Eburnean Event; U-Pb zircon geochronology.

Article History:
Received: 19/09/2024
Accepted: 05/03/2025
Published: 22/08/2025

Puntos clave:

Nuevas dataciones U-Pb indican que el Complejo Ígneo de Menongue se emplazó durante el Evento Eburneano entre 1982.4±22.9 y 1949.3±10.2 Ma.

El emplazamiento de las suites plutónica y volcánica del Complejo Ígneo de Menongue fue coetáneo.

RESUMEN

El Complejo Ígneo de Menongue (CIM), localizado en la Zona de Cassinga del Escudo de Angola, consiste en un conjunto de rocas plutónicas y volcánicas previamente no datadas. El complejo comprende esencialmente granodioritas y monzo- a sienogranitas en la suite plutónica, junto con rocas volcánicas andesíticas a riolíticas y depósitos piroclásticos en la suite volcánica. Nuevos datos geocronológicos de U-Pb en circón obtenidos durante el Plan Nacional de Geologia de Angola (PLANAGEO) revelan edades de cristalización entre 1982.4±22.9 Ma y 1949.3±10.2 Ma, demostrando que el magmatismo responsable por el emplazamiento del CIM ocurrió en el Paleoproterozóico, Durante el Evento Eburneano (ca. 2050 Ma a 1933 Ma en el Escudo de Angola). La superposición de las edades de cristalización de un monzogranito (1968.8±6.2 Ma) y de una riolita (1963.9±2.8 Ma) confirman evidencias de campo que sugieren emplazamiento coetáneo de las facies plutónicas y vulcánicas. Además, nuestros datos muestran que el magmatismo del CIM es coetáneo con los granitoides y las rocas volcánicas félsicas de Conda (noroeste de la Zona Central Eburneana: 1978±11 Ma a 1964±9 Ma), pero

Los datos refutan correlaciones previas con las rocas (sub)volcánicas de Matala (Zona de Cassinga) y Chibia-Cainde (Zona Central Eburneana).

descartan correlaciones previamente propuestas con las rocas (sub)volcánicas félsicas de Matala (Zona de Cassinga: 1440±6 Ma) y de Chibia-Cainde (sur de la Zona Eburneana Central: 1814±8 Ma a 1804±7 Ma). Futuros estudios detallados del registro Eburneano en la Zona de Cassinga (geoquímica de roca total y relaciones isotópicas U-Pb y Lu-Hf en circón) ayudarán a establecer la importancia geotectónica de la Zona de Cassinga en la evolución del supercontinente Columbia.

Palabras clave: Complejo Ígneo de Menongue; Zona de Cassinga; Escudo de Angola; Evento Eburneano; Geocronología U-Pb en circón.

Historial del artículo:
Recibido: 19/09/2024
Aceptado: 05/03/2025
Publicado: 22/08/2025

Citation / Cómo citar este artículo: Ferreira, E., Valverde-Vaquero, P., Gutíerrez-Medina, M., Buzzi-Marcos, J., Lopes, R., Gumiel, J.C., Merino-Martínez, E., Beranoaguirre, A., Feria, M.C., Montero, P., Manuel, J. (2025). Preliminary U-Pb Zircon Geochronology of the Eburnean Menongue Igneous Complex, Cassinga Zone, Angolan Shield. Boletín Geológico y Minero, 136(1), 006. http://doi.org/10.21701/bolgeomin/136.1/006.

1. Introduction

In recent years, the National Geological Plan of Angola (PLANAGEO) has focused on improving the geological knowledge of the country. The UTE PLANAGEO consortium, formed by the Instituto Geológico y Minero de España (IGME), the Laboratório Nacional de Geologia e Energia (LNEG) of Portugal, and Impulso Industrial Alternativo (IIAA), was responsible for geological, geophysical, and geochemical surveys in southern Angola.

The earliest mention of volcanic rock assemblages in central-south Angola dates back to Mouta (1933). Subsequent studies have revisited these rock suites, assigning them various designations such as "Cuchi–Serpa Pinto Volcanic Complex" (BRGM, 1970a), "Menongue Volcanic Complex" (Carvalho, 1981) or " Acid Volcanic and Subvolcanic Group " (Bassot *et al*., 1980/1981). These terms encompass the occurrence of volcanic and subvolcanic rocks that outcrop in a dispersed manner throughout the region between Cuchi, Menongue (formerly Serpa Pinto), and Caiundo. Despite being largely obscured by the sands of the Kalahari Group, the similarities in petrographic facies and magnetic signature suggest that these igneous rocks extend north of Menongue, towards Mumbué, and west-southwest of Caiundo, to the Mupa region, covering an area of over 10,000 km2 (Merino-Martínez *et al*., 2021 and references therein). The lithotypes range from basalts to rhyolites, with andesitic to rhyodacitic compositions the most common (BRGM, 1970a, b, c; Gumiel *et al*., 2021; Gutiérrez-Medina & Buzzi, 2021; Lopes *et al*., 2021; Sousa *et al*., 2021a, b; Buzzi & Gutiérrez-Medina, 2022). Mouta (1954) and the BRGM studies (1970b, c) describe gradual transitions between porphyries and granites, while Bassot *et al*. (1980/1981) report ambiguous relationships between granitoid and subvolcanic rocks in the Menongue area, where both are observed Cross-cutting each other. PLANAGEO's fieldwork in the Caiundo area confirmed these mutual cross-cutting relationships, indicating a contemporaneous formation of volcanic and plutonic facies (Lopes *et al*., 2021). Consequently, PLANAGEO integrated the plutonic facies, primarily biotite-amphibole granitoids previously defined and mapped as the Regional Granite (e.g.; Carvalho, 1981; Carvalho & Alves, 1993), with the volcanic and subvolcanic facies into a single igneous complex: the Menongue Igneous Complex. Earlier studies (e.g., BRGM, 1970b, c; Pascal, 1980; Carvalho & Alves, 1993; Pascal, 2006; Pereira *et al*., 2013), attempted to correlate the volcanic rocks of the Menongue Igneous Complex with other volcanic occurrences in central and southwestern Angola (e.g., Ganda, Matala, and/or Chibia-Cainde regions).

This study presents a preliminary assessment of the emplacement age of the Menongue Igneous Complex based on U-Pb data obtained during the PLANAGEO project. The analysed samples encompass volcanic and plutonic facies from the Menongue region, as well as a volcanic rock from the Mupa region, proposed as the southwestern extension of the Menongue Igneous Complex beneath the Kalahari sands.

2. Geological setting

The study area is located in central-southern Angola, within the Angolan Shield (AS), at the present southwestern margin of the Congo Craton. The Angolan Shield primarily outcrops in Angola, extending southward into northern Namibia and, to a lesser extent, northwestern Botswana. Within Angola, the Angolan Shield is divided into four main geotectonic zones (Ferreira *et al*., 2024 and references therein): the Central Shield Zone in the northeast, the Cassinga Zone in the southeast, the Central Eburnean Zone in the west, and the Namibe Zone in the southwest. The Namibe Zone extends southward to the Epupa Metamorphic Complex in northern Namibia. Further south, from west to east, lie the Sesfontein, Kamanjab, Grootfontein, Tsumkwe, and Quangwadum inliers (the latter in northwestern Botswana), collectively forming the southwestern margin of the Angolan Shield (Fig. 1).

The basement of the Angolan Shield is primarily composed of Paleoproterozoic igneous and metamorphic rocks of granitoid composition (Fig. 1; e.g., Seth, 1999; Carvalho *et al*., 2000; Hoal *et al*., 2000; Singletary *et al*., 2003; Kröner *et al*., 2004, 2010, 2015; Kröner, 2005; Luft *et al*., 2011; Pereira *et al*., 2011, 2013; Kleinhanns *et al*., 2013; McCourt *et al*., 2013; Jelsma *et al*., 2018). While these rocks exhibit a geological history dating back to the Mesoarchean, the most significant magmatic events occurred during the Paleoproterozoic and are interpreted as the product of collisional and/or accretionary orogenies, marked by intense magmatic and metamorphic activity at ca. 2050–1933 Ma (Eburnean), 1868–1830 Ma (Kamanjab), 1844–1790 Ma (Namibe), and 1790–1730 Ma (Epupa) (Jelsma *et al*., 2018; Ferreira *et al*., 2024). Following a ca. 200 My period of magmatic quiescence, activity in the southwestern Angolan Shield resumed in the Mesoproterozoic at ca. 1550 Ma and continued until ca. 1065 Ma, dominated by the emplacement of the Kunene Complex (ca. 1500–1360 Ma; e.g.: Bybee *et al*., 2019; Lehmann *et al*., 2020; Milani *et al*., 2022). The southern and southwestern margins of the AS were subsequently affected by the Pan-African orogeny (ca. 590–505 Ma; e.g.: Goscombe *et al*., 2017).

The Menongue Igneous Complex is part of the Cassinga Zone, one of the exposed Archean nuclei of the Angolan Shield (figs. 1 and 2). The Archean basement of the Cassinga Zone comprises the Jamba Group and the Jamba-Tchamutete Plutonic Suite. The Jamba Group is a highly deformed metavolcanic-sedimentary sequence interlayered with banded iron formations and metamorphosed under greenschist facies conditions (Kopershoek, 1970, 1984; Pascal, 1980; Bassot *et al*., 1980/1981; Sousa *et al*., 2021a, b; Buzzi & Gutiérrez-Medina, 2022). This sequence is associated with granitoids of the Jamba-Tchamutete Plutonic Suite, dated between 2667 ± 15 Ma and 2568 ± 7 Ma (Merino-Martínez *et al*., under review). The Chivanda Group, a pre- to syn-Eburnean metavolcanosedimentary sequence, unconformably overlies the Neoarchean units of the Cassinga Zone (Sousa *et al*., 2021a, b; Buzzi & Gutiérrez-Medina, 2022 and references therein). These units underwent deformation and metamorphism during the Eburnean Event (2.05–1.93 Ga), accompanied by the emplacement of the Cuvelai–Matala Granitic Suite (1982 ± 8 Ma; Merino-Martínez *et al*., under review) and the intermediate to felsic plutonic and (sub)volcanic rocks of the Menongue Igneous Complex (Gumiel *et al*., 2021; Gutiérrez-Medina & Buzzi, 2021; Lopes *et al*., 2021; Sousa *et al*., 2021a, b; Buzzi & Gutiérrez-Medina, 2022). These geological units are overlain by the siliciclastic Bale Group, a relatively undeformed sedimentary sequence interpreted as a potential Eburnean molasse (e.g., Bassot *et al*., 1980/1981; Pereira *et al*., 2021) (Fig. 2).

The Menongue Igneous Complex outcrops in a scattered manner in the eastern and southern parts of the Cassinga Zone, exposed by the incision of the present-day river network into the overlying Kalahari Group sands. Major exposures occur in the Cuchi–Menongue–Caiundo area, with smaller outcrops extending southwest towards Mupa (Fig. 2). PLANAGEO's geological mapping divides the complex into Plutonic and Volcanic Suites. The Plutonic Suite is predominantly composed of equigranular, medium- to fine-grained granodiorites and monzogranites, seldom exhibiting porphyritic texture. These rocks consist mainly of quartz, K-feldspar, plagioclase, biotite, and amphibole, with magnetite and sphene as common accessory minerals (figs. 3A and B). Rounded mafic microgranular enclaves occur locally (Fig. 3C). Compositionally more evolved leucogranites (figs. 3D-F), as well as less evolved diorites (Fig. 3G), quartz diorites, and tonalites are subordinate (Gutiérrez-Medina & Buzzi, 2021; Lopes *et al*., 2021; Sousa *et al*., 2021a, b; Buzzi & Gutiérrez-Medina, 2022). The rocks are strongly magnetic and usually undeformed, contrasting with the typically deformed, weakly to non-magnetic Neoarchean granitoids of the Jamba-Tchamutete Plutonic Suite (Sousa *et al*., 2021a, b; Buzzi & Gutiérrez-Medina, 2022).

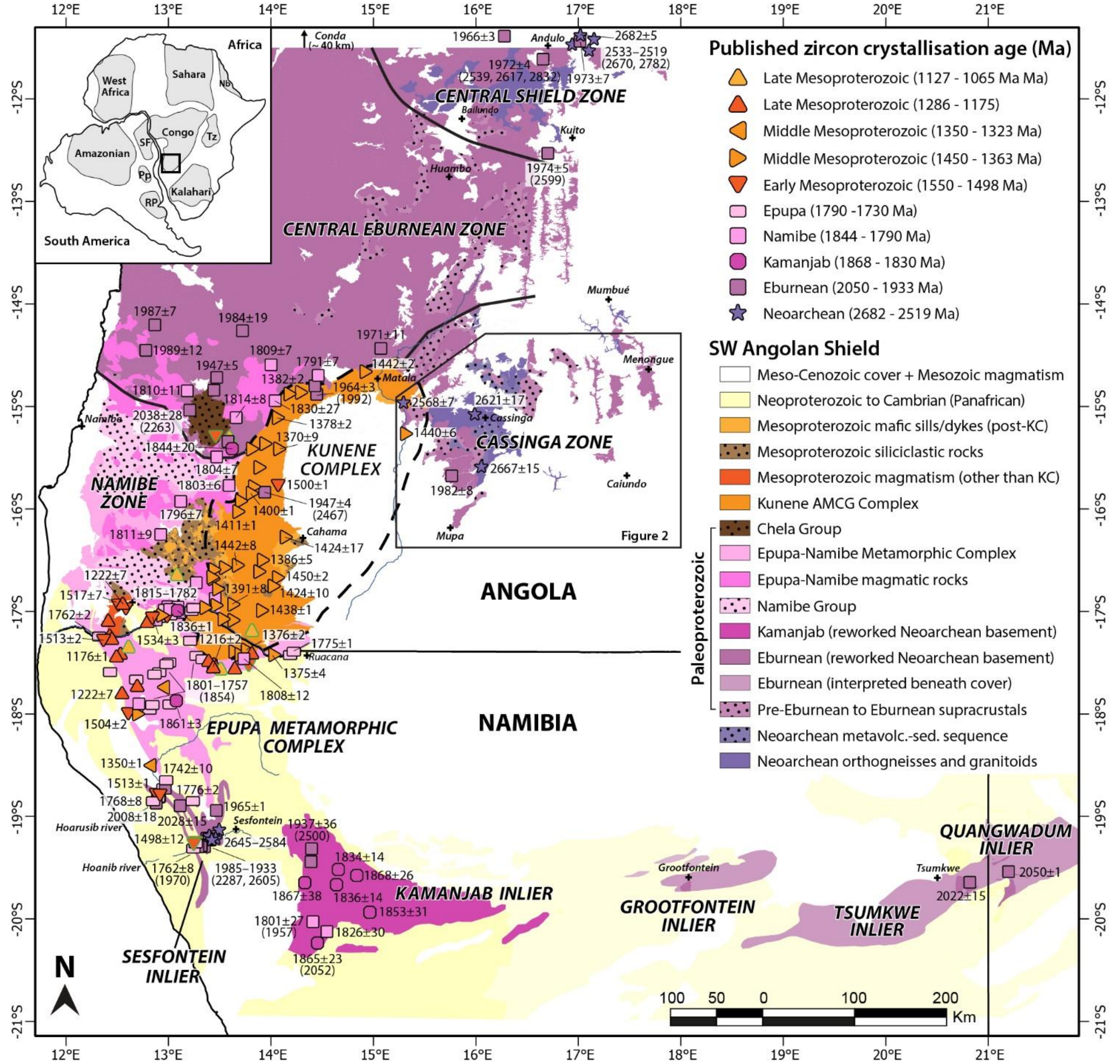

Figure 1. Geological map showing the Precambrian geotectonic domains of the Angolan Shield of NW Namibia and SW Angola and published U-Pb zircon crystallization ages (modified from Ferreira *et al*., 2024). Inherited zircon U-Pb ages are indicated in parentheses. The dashed line of the Kunene Complex corresponds to the limits of the complex as interpreted from gravimetric (Rey-Moral *et al*., 2022) and magnetic (Rodrigues *et al*., 2021) geophysical data. The inset shows the position of the Congo craton relative to other African and South American cratons in a reconstruction of West Gondwana prior to Mesozoic Pangea breakup. The location of the study area is indicated by the black polygon.

Figura 1. Mapa geológico de los dominios geotectónicos precámbricos del Escudo de Angola en el NW de Namibia y SW de Angola, con edades de cristalización U-Pb en circón publicadas (modificado de Ferreira *et al*., 2024). Las edades heredadas se indican entre paréntesis. La línea discontinua del Complejo del Kunene corresponde a los límites del complejo tal como se interpreta a partir de los datos geofísicos gravimétricos (Rey-Moral *et al*., 2022) y magnéticos (Rodrigues *et al*., 2021). El recuadro muestra la posición del cratón del Congo en relación con otros cratones africanos y sudamericanos en una reconstrucción de Gondwana Occidental antes de la ruptura de Pangea en el Mesozoico. La localización del área de estudio está indicada por el polígono negro.

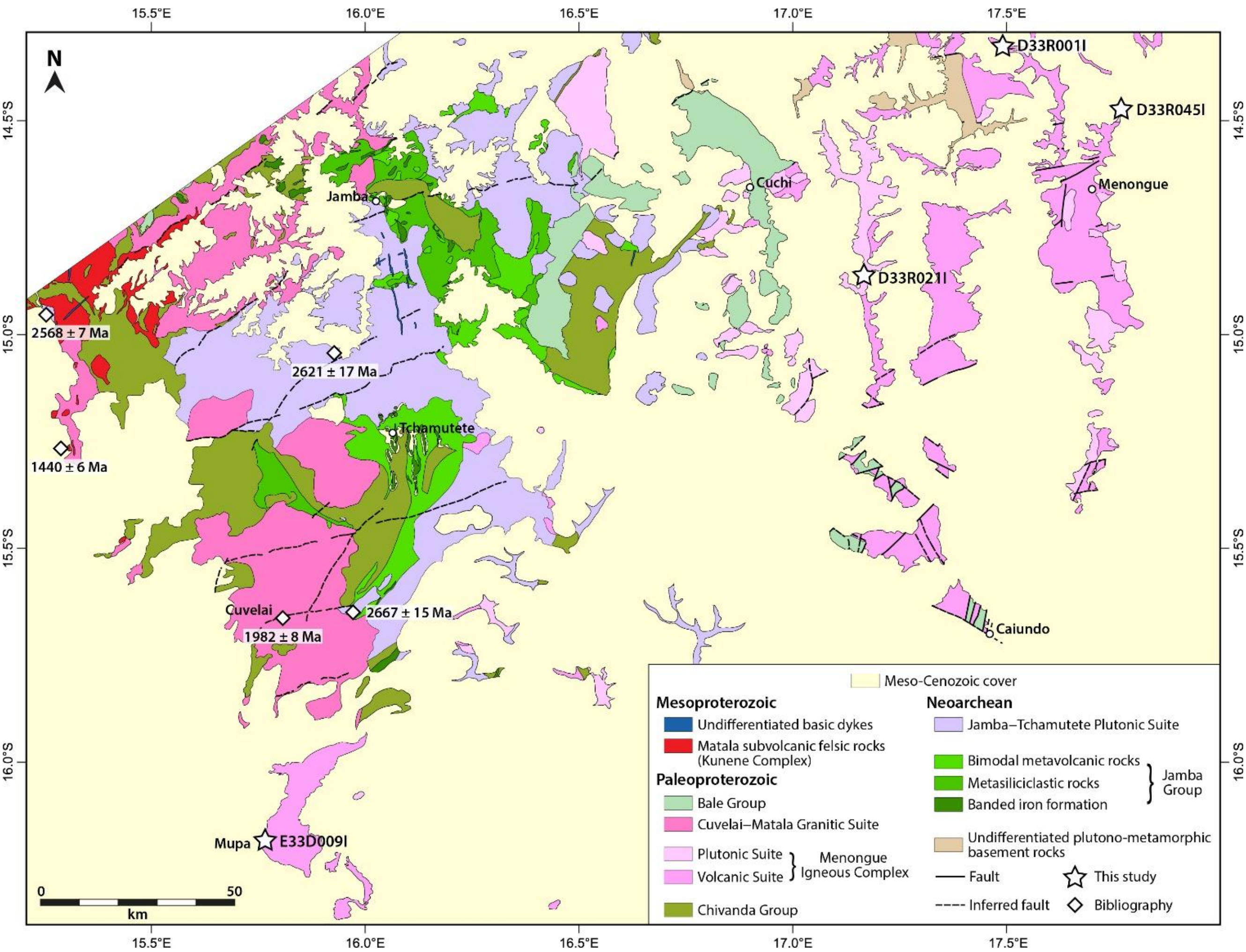

Figure 2. Geological map of the study area modified from the geological map of Angola at 1:1.000.000 scale of the Geological Institute of Angola (Merino-Martínez *et al*., 2021). Reported U-Pb crystallization ages are from Merino-Martínez *et al*., under review.

Figura 2. Mapa geológico del área de estudio modificado a partir del mapa geológico de Angola a escala 1:1.000.000 del Instituto Geológico de Angola (Merino-Martínez *et al*., 2021). Las edades de cristalización U-Pb reportadas son de Merino-Martínez *et al*. (en revisión).

The Volcanic Suite comprises coherent volcanic and subvolcanic rocks of predominantly dacitic to rhyodacitic composition, although andesitic and rhyolitic varieties also occur. They are characterized by a dark-reddish or grey to black crypto- to microcrystalline matrix containing variable proportions of phenocrysts of potassium feldspar, plagioclase, and, in lesser amounts, quartz, amphibole, and/or biotite. Magmatic flow structures are common (BRGM, 1970a, b, c; Gumiel *et al*., 2021; Gutiérrez-Medina & Buzzi, 2021; Lopes *et al*., 2021; Sousa *et al*., 2021a; Buzzi & Gutiérrez-Medina, 2022) (Fig. 4A-E). Volcaniclastic rocks are also present and are classified as pyroclastic pyroclastic- and tuff breccias, ash-tuffs and ignimbrites, consisting primarily of volcanic lithoclasts and pumice fragments embedded in a micro- to cryptocrystalline siliceous matrix. Phenocrysts of potassium feldspar, quartz, amphibole, and/or pyroxene are also present within the siliceous matrix, occasionally along with deformed glass fragments (fiamme). These well-consolidated deposits share a similar composition with the surrounding volcanic rocks and indicate high-energy, subaerial eruptive volcanic processes (BRGM, 1970 b, c; Gutiérrez-Medina & Buzzi, 2021; Lopes *et al*., 2021) (Fig. 4F).

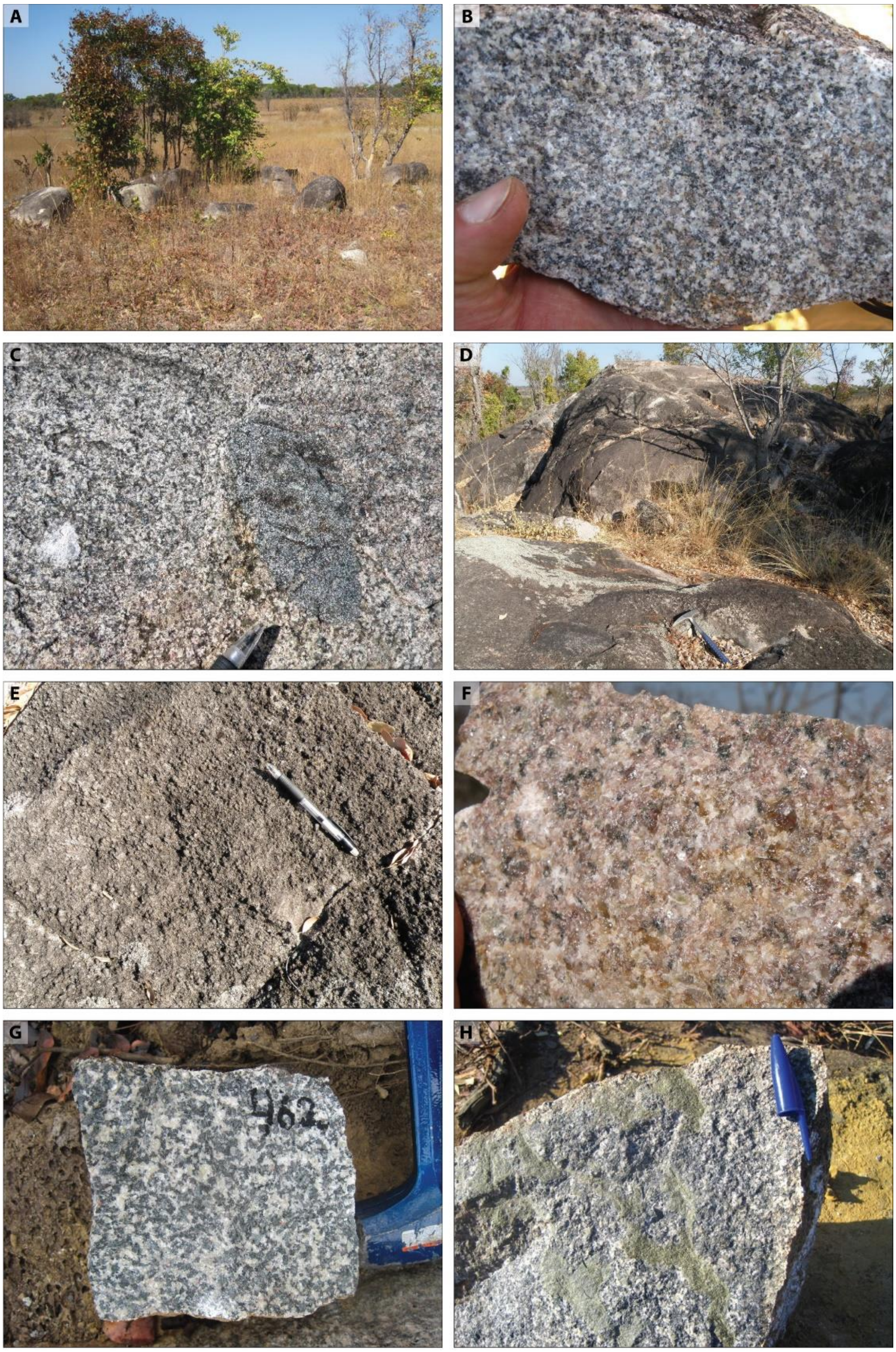

Figure 3. Representative field photographs of the Plutonic Suite of the Menongue Igneous Complex (MIC). A) Outcrop view showing the sampling location of the dated biotite-amphibole monzogranite (D33R021I). The MIC is characterized by scattered outcrops of small dimensions. B) Closer view of the isotropic, medium-grained, biotite-hornblende monzogranite. C) Rounded mafic enclave within a granitoid. D) Outcrop view of the sampling location of the dated syenogranite (D33R045I). E) Detail of the syenogranite showing a subtle foliation parallel to the pencil line F) Closer view of the syenogranite. G) Diorite. H) Granitoid displaying fracture-controlled propylitic alteration.

Figura 3. Fotografías de campo representativas de la Suite Plutónica del Complejo Ígneo de Menongue (CIM). A) Afloramiento del punto de muestreo del monzogranito con biotita y hornblenda datado (D33R021I). El CIM se caracteriza por afloramientos dispersos de pequeñas dimensiones. B) Detalle del monzogranito con biotita y hornblenda. C) Enclave máfico en granitoide. D) Afloramiento del punto de muestreo del sienogranito datado (D33R045I). E) Detalle del sienogranito donde se observa una ligera foliación (paralela al portaminas). F) Detalle del sienogranito. G) Diorita. H) Granitoide con alteración propilítica controlada por fractura.

Figure 4. Representative field photographs of the Volcanic Suite of the Menongue Igneous Complex (MIC). A) Outcrop view showing the sampling location of the dated porphyritic dacite (D33R001I). B) Closer view of the porphyritic dacite with feldspar and quartz phenocrysts embedded in a dark-grey aphanitic matrix. Note the presence of epidotized feldspar-rich domains. C) Quarry where the dated porphyritic rhyolite (E33D009I) was collected. D) Porphyry with feldspar, biotite, amphibole and minor quartz phenocrysts embedded in a dark-grey microcrystalline matrix. E) Felsic lava displaying a banded texture of volcaniclastic material composed of small quartz and feldspar fragments. F) Pyroclastic deposit containing elongated dark-grey volcanic lithoclasts and white to cream-colored pumice fragments, embedded in a lighter grey stratified tuffaceous matrix. G) Porphyritic dacite with fracture-controlled propylitic alteration. H) Felsic porphyry exhibiting pervasive hematitization.

Figura 4. Fotografías de campo representativas de la Suite Volcánica del Complejo Ígneo de Menongue (CIM). A) Afloramiento del punto de muestreo de la dacita porfírica datada (D33R001I). B) Detalle de la dacita porfírica con fenocristales de feldespato y cuarzo en una matriz afanítica gris oscuro. Se observa la presencia de dominios anhedrales ricos en feldespato epidotizado. C) Cantera donde se muestreó la riolita porfídica datada (E33D009I). D) Pórfido con fenocristales de feldespato, biotita, anfíbol y, en menor medida, cuarzo en una matriz microcristalina gris oscuro. E) Lava félsica con textura bandeada, compuesta por fragmentos de feldespato y cuarzo. F) Depósito piroclástico con litoclastos volcánicos de color gris oscuro y fragmentos de pumita de color blanco a crema elongados en una matriz tufácea estratificada de color gris más claro. G) Dacita porfídica con alteración propilítica controlada por fracturas. H) Pórfido félsico hematitizado.

The plutonic and volcanic suites locally exhibit significant hydrothermal alteration, characterized by silicification, hematitization, epidotization, and/or chloritization (figs. 3H, 4G-H), along with recrystallization resulting from contact metamorphism caused by nearby intrusions. There is no evidence of regional metamorphism (BRGM, 1970a, b, c; Gumiel *et al*., 2021; Gutiérrez-Medina & Buzzi, 2021; Lopes *et al*., 2021; Sousa *et al*., 2021a).

3. U-Pb zircon geochronology

3.1. Sampling

Four magmatic samples from the Menongue Igneous Complex were collected for U-Pb zircon geochronology: two from the Plutonic Suite and two from the Volcanic Suite (Fig. 2).

Sample D33R045I is a slightly foliated medium- to coarse-grained syenogranite (leucogranite), containing rare subhedral to anhedral K-feldspar phenocrysts (Fig. 3E-F). It was collected approximately 20 km northeast of Menongue along the Cuebe river (14.499°S, 17.765°E).

Sample D33R021I, collected along the Luassenha river, approximately 35 km southeast of Cuchi (14.859°S, 17.169°E), is an isotropic, medium-grained, biotite-hornblende monzogranite containing accessory sphene and magnetite (Fig. 3B).

Sample D33R001I (14.328°S, 17.488°E) is a porphyritic dacite containing small quartz and feldspar phenocrysts with corrosion gulfs, embedded in a dark-grey aphanitic matrix (Fig. 4B). Scattered epidotized feldspar-rich domains, up to five centimeters in size, are also observed. This sample was collected along a tributary of the Cuebe river, approximately 45 km north-northwest of Menongue.

Sample E33D009I (16.181°S, 15.759°E), collected in a quarry near Mupa (Fig. 4C), is a porphyritic rhyolite characterized by very small phenocryst of feldspar, quartz, and minor amphibole embedded in a black aphanitic matrix.

3.2. Analytical methods: SHRIMP and CA-ID-TIMS

Zircon mineral separation was performed at IGME laboratories in Tres Cantos (Spain) following a modified version of the “water-based” mineral separation procedure of Söderlund & Johansson (2002), with further concentration using a Frantz isodynamic magnetic separator. Finally, selected zircons were hand-picked under a binocular microscope.

The U-Pb SHRIMP IIe/mc zircon analyses were performed at the IBERSIMS facility of the University of Granada (Spain) following the method described by Williams & Claesson (1987). The hand-picked zircons of each sample were cast in a 3.5 cm diameter epoxy mount (megamount) along with several grains of the TEMORA-1 zircon, used as isotope ratios standard (416.8 ± 1.1 Ma; Black et al., 2003), one grain of the SL13 zircon, used as a concentration standard (238 ppm U; Claoué-Long et al., 1995), and a few grains of the REG zircon (ca. 2.5 Ga, very high U, Th and common lead content), used for mass calibration. The mount was polished and documented using optical (reflected and transmitted light) and scanning electron microscopy (secondary electrons and cathodoluminescence). After extensive cleaning and drying, the mount was coated with ultra-pure gold (8–10 nm thick). Each spot was rastered with the primary beam for 120 s prior to the analysis, and then analysed for 6 scans, following the isotope peak sequence $^{196}Zr_2O$, ^{204}Pb, 204.1background, ^{206}Pb, ^{207}Pb, ^{208}Pb, ^{238}U, ^{248}ThO, ^{254}UO. Each peak of every scan was measured sequentially 10 times with the following total counting times per scan: 2 s for mass 196; 5 s for masses 238, 248, and 254; 15 s for masses 204, 206, and 208; and 20 s for mass 207. The primary beam, composed of 16O−16O+, was set to an intensity of about 5 nA, with a 120 µm Kohler aperture, which generated 17 × 20 µm elliptical spots on the target. The secondary beam exit slit was fixed at 80 µm, achieving a resolution of about 5000 at 1% peak height. All calibration procedures were performed on the standards included on the same mount. The analytical session started measuring the SL13 zircon, with TEMORA-1 zircon then measured every 4 unknowns. Data reduction was done with the SHRIMPTOOLS software (available at https://www.ugr.es/~fbea/software.html, which is a new implementation of the original PRAWN software developed for the SHRIMP. Errors are reported at the 95% confidence interval. Errors on the replicates of the TEMORA standard measured during the analytical session were ±0.19% for $^{206}Pb/^{238}U$ and ±0.27% for $^{207}Pb/^{206}Pb$. Further details on calibration and data reduction procedures are available on the IBERSIMS website (https://www.ugr.es/~ibersims/ibersims/Zircon_Oxygen_Isotopes_analysis_files/SHRIMP_geocron_method.pdf).

The U–Pb CA-ID-TIMS zircon analysis was made at the IGME laboratories. Zircons were pre-treated with the chemical abrasion method of Mattinson (2005), followed by annealing at 950°C for 48 hours and attacked with HF+8HNO3 at 180°C for 12 hours. Before final dissolution in Parrish-type mini bombs, the samples were spiked with a ^{205}Pb-^{233}U-^{235}U spike (spike BSU-1B, courtesy of the MIT laboratory). U and Pb chemical separation followed the method of Krogh (1973) using a down-sized column. Isotopic relationships were measured with a Triton multicollector TIMS mass spectrometer equipped with an axial secondary multiplier ion counter. Pb was measured in the 1300-1500°C temperature range and U was measured as dioxide at temperatures between 1450 and 1600°C. The linearity and dead-time correction of the SEM were checked using the U500 and NBS982 standards. The artificial Earthtime 500 Ma solution was used to test the calibration of the spike and the oxide correction of the U measurements with the triple spike. Results assure accuracy within 0.1%. The data was processed using the PbMacDat spreadsheet (Isachsen et al., 2007). All reported isotopic ratios are corrected for mass fractionation (Pb 0.11±0.02% AMU, U 0.10 ± 0.02%), blank (2-5 pg Pb, 0.1 pg U) and initial common Pb using the model of Stacey & Kramers (1975). For further details regarding U-Pb dating by CA-ID-TIMS at IGME laboratories see Valverde-Vaquero (2009).

Concordia diagrams and age calculations were performed using IsoplotR v.6.3 (Vermeesch, 2018). Data point ellipses and age uncertainties are reported at 95% confidence level. Tables 1 to 4 summarise the U-Pb isotopic results obtained for the analysed samples.

3.3. Results

Eighteen U-Pb SHRIMP analyses were conducted on sixteen zircons from sample D33R045I (syenogranite) (Table 1). Seventeen of these analyses (Fig. 5A) yield an upper intercept age of 1976.4 ± 23.9 Ma (MSWD = 0.43, ρ = 0.97) and a lower intercept age of 464 ± 62 Ma. The upper intercept age is indistinguishable, within uncertainty, from the Concordia age of 1982.4 ± 22.9 Ma (MSWD = 0.24, ρ = 0.98) obtained from four (sub)concordant analyses, interpreted as the crystallization age of the syenogranite. An inherited core displays a concordia age of 2672 ± 66 Ma.

Sixteen U-Pb SHRIMP analyses were made on sixteen zircons from sample D33R021I (monzogranite) (Table 2). Regression of all data (Fig. 5B) provide an upper intercept age of 1969.9 ± 10.2 Ma (MSWD = 0.34, ρ = 0.99) and a lower intercept age of 472 ± 119 Ma. The upper intercept age is identical, within uncertainty, to the Concordia age of 1968.8 ± 6.2 Ma (MSWD = 1.1, ρ = 0.32) obtained from eight (sub)concordant analyses, interpreted as the crystallization age of the monzogranite.

Sixteen U-Pb SHRIMP analyses were performed on sixteen zircons from sample D33R001I (dacite) (Table 3). Regression of twelve of these analyses (Fig. 5C) yield an upper intercept age of 1945.6 ± 21.6 Ma (MSWD = 0.52, ρ = 0.88) and a lower intercept age of 568 ± 101 Ma. The upper intercept age is indistinguishable, within uncertainty, from the Concordia age of 1949.3 ± 10.2 Ma (MSWD = 0.58, ρ = 0.87) obtained from seven (sub)concordant analyses, interpreted as the crystallization age of the dacite. Three analysed zircons provide an upper intercept age of 2048.2 ± 24.1 Ma (MSWD = 0.41, ρ = 0.52), while another one exhibits a concordia age of 2091 ± 20 Ma. These zircons display internal textures and $^{232}Th/^{238}U$ ratios identical to the main zircon population, suggesting a xenocrystic origin.

U–Pb analyses for sample E33D009I (rhyodacite) (Table 4) were conducted by CA-ID-TIMS and carried out on three fractions of zircon, each comprising between 4 and 5 crystals. Free regression of the data for all three fractions results in a lower intercept within error of the origin, suggesting only recent Pb-loss; therefore, a linear regression was anchored at 0 Ma, providing an upper intercept age of 1963.9 ± 2.8 Ma (MSWD = 1.57, ρ = 0.21; Fig. 5D), interpreted as the crystallisation age of the volcanic rock.

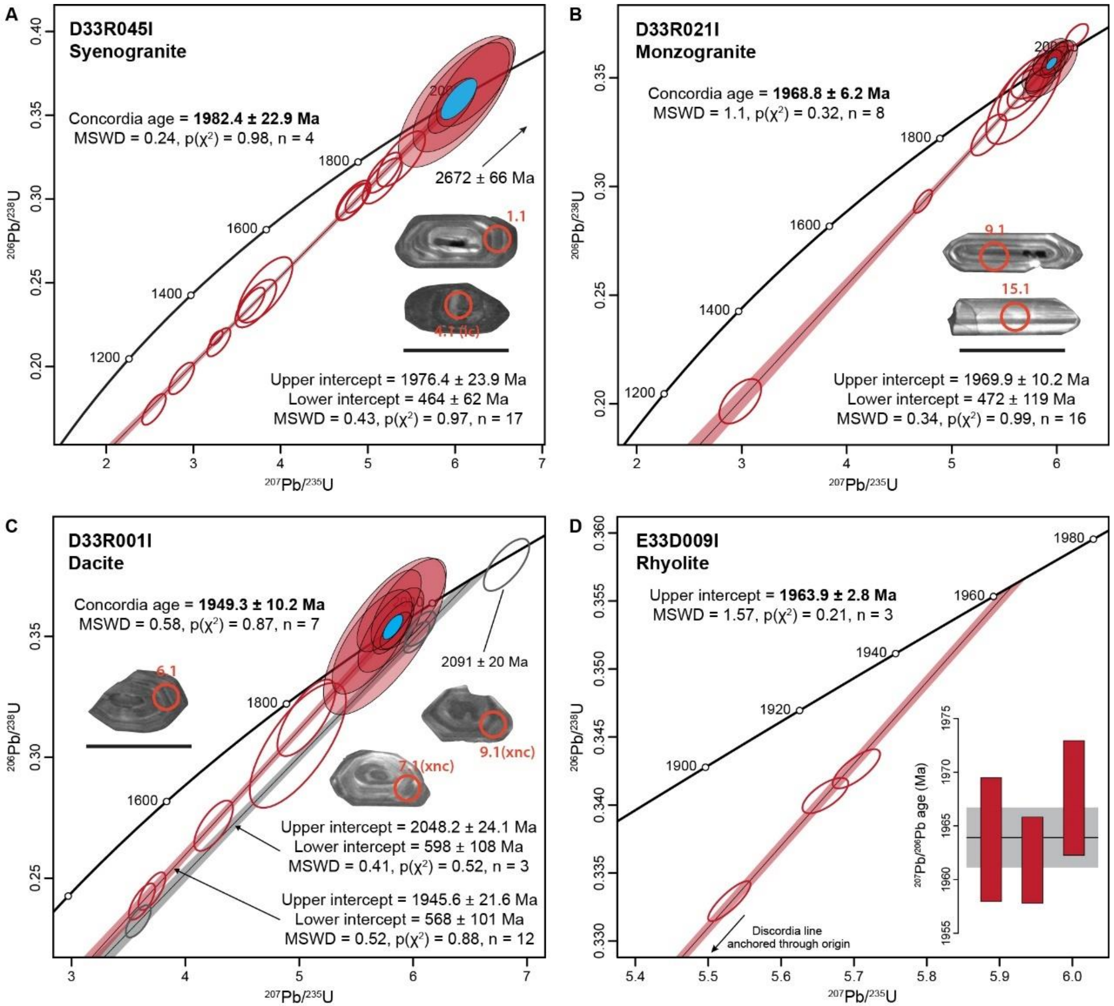

Figure 5. Concordia diagrams for the studied samples: A) D33R045I (syenogranite), B) D33R021I (monzogranite), C) D33R001I (dacite), and D) E33D009I (rhyolite). The Concordia ages are indicated by the blue ellipses (calculated using only data from the red-filled ellipses). Representative CL images of the analysed zircons are provided in figures 5A, B, and C (scale bar = 100 µm.IC: inherited core; xnc: xenocryst).

Figura 5. Diagramas Concordia para las muestras estudiadas: A) D33R045I (sienogranito), B) D33R021I (monzogranito), C) D33R001I (dacita) y D) E33D009I (riolita). Las edades de Concordia están indicadas por las elipses azules (calculadas utilizando solo los datos de las elipses rojas rellenas). Imágenes representativas en CL de los circones analizados se proporcionan en las figuras 5A, B y C (barra de escala = 100 µm. IC: núcleo heredado; xnc: xenocristal).

D33R045I (syenogranite)						Isotopic Ratios							Ages (Ma)						
Spot #	U (ppm)	Th (ppm)	^{232}Th/^{238}U	^{206}Pb* (ppm)	^{206}Pb$_c$ (%)	^{207}Pb/^{235}U	±	^{206}Pb/^{238}U	±	Rho	^{207}Pb/^{206}Pb*	±	^{207}Pb/^{235}U	±	^{206}Pb/^{238}U	±	^{207}Pb/^{206}Pb	±	Conc. distance (%)
1.1	553	474	0.88	171	0.22	5.969	0.113	0.356	0.007	0.72	0.1217	0.0017	1971	17	1962	32	1981	25	+1.0
2.1	428	357	0.85	134	0.25	6.070	0.227	0.361	0.013	0.71	0.1220	0.0034	1986	33	1986	63	1986	50	+0.0
3.1	389	423	1.12	121	0.22	6.010	0.270	0.358	0.016	0.72	0.1217	0.0041	1977	39	1973	76	1982	60	+0.2
4.1	332	324	1.00	145	0.41	12.770	0.483	0.502	0.019	0.72	0.1844	0.0052	2663	36	2623	81	2693	47	+1.6
5.1	444	963	2.22	142	0.08	6.238	0.185	0.370	0.011	0.71	0.1224	0.0027	2010	26	2028	51	1991	40	-0.9
6.1	1281	1110	0.89	195	0.72	2.547	0.056	0.174	0.004	0.71	0.1059	0.0017	1286	16	1037	21	1730	30	+19.1
7.1	1014	225	0.23	264	0.06	4.886	0.059	0.301	0.004	0.71	0.1179	0.0011	1800	10	1694	18	1924	16	+5.9
7.2	616	147	0.25	160	0.11	4.832	0.080	0.299	0.005	0.70	0.1171	0.0015	1790	14	1687	24	1913	23	+5.7
8.1	689	549	0.82	186	0.30	5.165	0.093	0.311	0.006	0.72	0.1206	0.0016	1847	15	1744	27	1964	24	+5.6
9.1	748	69	0.10	193	0.08	4.829	0.073	0.298	0.004	0.71	0.1173	0.0013	1790	13	1684	22	1916	20	+5.9
10.1	717	314	0.45	136	0.66	3.263	0.029	0.217	0.002	0.64	0.1090	0.0008	1472	7	1267	9	1783	13	+13.8
11.1	1092	506	0.48	187	2.49	2.862	0.059	0.193	0.004	0.70	0.1076	0.0017	1372	15	1137	21	1759	29	+16.7
12.1	718	1415	2.02	197	0.22	5.182	0.082	0.316	0.005	0.71	0.1190	0.0014	1850	14	1769	24	1942	22	+4.4
13.1	748	1101	1.51	156	1.25	3.715	0.096	0.238	0.006	0.68	0.1134	0.0023	1575	21	1374	30	1854	36	+12.4
14.1	1161	1372	1.21	220	2.18	3.291	0.054	0.215	0.003	0.70	0.1112	0.0014	1479	13	1253	18	1820	23	+14.9
15.1	993	1128	1.17	204	0.25	3.663	0.063	0.237	0.004	0.72	0.1120	0.0014	1563	14	1373	21	1832	23	+12.1
16.1	536	160	0.31	150	0.02	5.381	0.113	0.324	0.007	0.72	0.1205	0.0019	1882	18	1809	33	1963	28	+3.9
16.2	1282	542	0.43	273	0.14	3.822	0.128	0.246	0.008	0.70	0.1128	0.0029	1597	27	1417	41	1844	46	+11.1

Errors are at 1σ level; the error in ^{206}Pb/^{238}U averaging the standard has been already propagated.
Point-to point errors, calculated on replicates of the TEMORA standard, are: 0.20 % for ^{206}Pb/^{238}U, and 0.39 % for ^{207}Pb/^{206}Pb.
Isotopic data are ^{204}Pb corrected

Table 1. Zircon U-Pb SHRIMP isotopic data for sample D33R045I (syenogranite).

Tabla 1. Datos isotópicos U-Pb SHRIMP en circón para la muestra D33R045I (sienogranito).

D33R021I (monzogranite)						**Isotopic Ratios**							**Ages (Ma)**						
Spot #	**U (ppm)**	**Th (ppm)**	**^{232}Th/^{238}U**	**^{206}Pb* (ppm)**	**^{206}Pb$_c$ (%)**	**^{207}Pb/^{235}U**	**±**	**^{206}Pb/^{238}U**	**±**	**Rho**	**^{207}Pb/^{206}Pb***	**±**	**^{207}Pb/^{235}U**	**±**	**^{206}Pb/^{238}U**	**±**	**^{207}Pb/^{206}Pb**	**±**	**Conc. distance (%)**
1.1	132	213	1.66	42	0.01	6.193	0.044	0.370	0.002	0.59	0.1215	0.0007	2003	6	2028	10	1978	11	-1.2
2.1	96	161	1.72	30	0.06	6.010	0.061	0.359	0.003	0.62	0.1213	0.0010	1977	9	1979	15	1976	15	-0.1
3.1	700	73	0.11	178	0.25	4.726	0.036	0.293	0.002	0.71	0.1169	0.0007	1772	6	1657	11	1910	10	+6.4
4.1	912	1334	1.50	162	1.97	2.986	0.081	0.201	0.004	0.55	0.1076	0.0025	1404	21	1182	23	1760	43	+18.0
5.1	236	542	2.35	66	0.61	5.352	0.069	0.324	0.004	0.67	0.1199	0.0012	1877	11	1808	19	1955	18	+3.6
6.1	161	289	1.84	48	0.17	5.713	0.074	0.346	0.004	0.67	0.1197	0.0012	1933	11	1917	20	1951	18	+0.8
7.1	220	666	3.11	68	0.03	5.941	0.069	0.360	0.003	0.60	0.1198	0.0012	1967	10	1980	17	1954	17	-0.6
8.1	83	166	2.04	25	0.18	5.694	0.103	0.345	0.006	0.69	0.1197	0.0017	1931	16	1911	29	1951	25	+1.0
9.1	191	351	1.89	59	0.28	5.981	0.056	0.357	0.003	0.64	0.1214	0.0009	1973	8	1969	14	1977	14	+0.2
10.1	118	197	1.71	35	0.06	5.833	0.064	0.347	0.003	0.63	0.1218	0.0011	1951	10	1921	16	1983	16	+1.5
11.1	113	219	1.98	35	0.03	6.004	0.040	0.361	0.002	0.68	0.1207	0.0006	1976	6	1986	11	1967	9	-0.5
12.1	61	86	1.45	19	0.41	5.873	0.071	0.353	0.004	0.69	0.1207	0.0011	1957	11	1949	20	1967	17	+0.4
13.1	132	243	1.89	39	0.16	5.683	0.145	0.340	0.009	0.71	0.1211	0.0023	1929	22	1889	41	1972	35	+2.1
14.1	39	41	1.08	12	0.30	5.951	0.100	0.354	0.005	0.65	0.1218	0.0017	1969	15	1955	26	1983	24	+0.7
15.1	68	94	1.42	21	0.25	5.743	0.072	0.347	0.003	0.47	0.1199	0.0014	1938	11	1922	14	1955	20	+0.8
16.1	145	106	0.75	44	0.17	5.874	0.084	0.353	0.004	0.55	0.1206	0.0015	1957	12	1950	19	1965	22	+0.3

Errors are at 1σ level; the error in ^{206}Pb/^{238}U averaging the standard has been already propagated.
Point-to point errors, calculated on replicates of the TEMORA standard, are: 0.20 % for ^{206}Pb/^{238}U, and 0.39 % for ^{207}Pb/^{206}Pb.
Isotopic data are ^{204}Pb corrected

Table 2. Zircon U-Pb SHRIMP isotopic data for sample D33R021I (monzogranite).

Tabla 2. Datos isotópicos U-Pb SHRIMP en circón para la muestra D33R021I (monzogranito).

D33R001I (dacite)								Isotopic Ratios								Ages (Ma)			
Spot #	U (ppm)	Th (ppm)	$^{232}Th/^{238}U$	$^{206}Pb^*$ (ppm)	$^{206}Pb_c$ (%)	$^{207}Pb/^{235}U$	±	$^{206}Pb/^{238}U$	±	Rho	$^{207}Pb/^{206}Pb^*$	±	$^{207}Pb/^{235}U$	±	$^{206}Pb/^{238}U$	±	$^{207}Pb/^{206}Pb$	±	Conc. Distance (%)
1.1	1095.9	580.8	0.54	232.8	0.37	3.705	0.049	0.2446	0.0032	0.71	0.1099	0.0011	1573	11	1411	17	1797	18	+10.1
2.1	531.4	537.8	1.04	162.3	0.06	5.805	0.118	0.3527	0.0072	0.72	0.1194	0.0018	1947	18	1947	34	1947	27	-0.0
3.1	595.7	965.3	1.66	163.4	0.19	5.063	0.104	0.3164	0.0065	0.72	0.1161	0.0018	1830	17	1772	32	1897	28	+3.2
4.1	770.3	469.0	0.62	181.8	0.39	4.247	0.070	0.2717	0.0043	0.69	0.1134	0.0014	1683	13	1549	22	1854	23	+7.9
5.1	343.3	368.2	1.10	105.1	0.00	5.826	0.074	0.3536	0.0044	0.72	0.1195	0.0011	1950	11	1952	21	1949	17	-0.1
6.1	404.7	296.6	0.75	124.3	0.82	5.847	0.056	0.3524	0.0031	0.67	0.1203	0.0009	1953	8	1946	15	1961	14	+0.4
7.1	328.0	240.6	0.75	107.9	0.08	6.820	0.082	0.3796	0.0044	0.70	0.1303	0.0012	2088	11	2075	21	2102	16	+0.7
7.2	402.6	248.9	0.63	106.7	0.48	4.988	0.173	0.3050	0.0106	0.72	0.1186	0.0031	1817	29	1716	52	1936	47	+5.6
8.1	619.6	402.4	0.67	125.6	0.99	3.588	0.045	0.2321	0.0027	0.68	0.1121	0.0011	1547	10	1346	14	1834	18	+12.7
9.1	235.0	200.8	0.88	71.9	0.11	6.064	0.054	0.3532	0.0029	0.67	0.1245	0.0009	1985	8	1950	14	2022	12	+1.8
10.1	429.3	225.4	0.54	130.0	0.10	6.031	0.047	0.3497	0.0026	0.70	0.1251	0.0007	1980	7	1933	13	2030	10	+2.3
11.1	232.8	313.6	1.38	70.6	0.09	5.749	0.219	0.3501	0.0133	0.72	0.1191	0.0034	1939	33	1935	63	1942	51	+0.2
12.1	146.1	175.6	1.23	46.0	0.01	5.961	0.135	0.3633	0.0077	0.67	0.1190	0.0021	1970	20	1998	36	1941	32	-1.4
13.1	360.0	339.1	0.97	108.4	0.05	5.640	0.144	0.3478	0.0088	0.72	0.1176	0.0023	1922	22	1924	42	1920	34	-0.1
14.1	730.9	552.2	0.78	152.6	0.45	3.618	0.047	0.2403	0.0031	0.71	0.1092	0.0011	1554	10	1388	16	1786	18	+10.4
15.1	170.4	97.5	0.59	53.2	0.01	5.789	0.116	0.3606	0.0069	0.69	0.1164	0.0018	1945	17	1985	33	1902	28	-2.1

Errors are at 1σ level; the error in $^{206}Pb/^{238}U$ averaging the standard has been already propagated.
Point-to point errors, calculated on replicates of the TEMORA standard, are: 0.20 % for $^{206}Pb/^{238}U$, and 0.39 % for $^{207}Pb/^{206}Pb$.
Isotopic data are ^{204}Pb corrected

Table 3. Zircon U-Pb SHRIMP isotopic data for sample D33R001I (dacite).

Tabla 3. Datos isotópicos U-Pb SHRIMP en circón para la muestra D33R001I (dacita).

E33D009I (rhyodacite)								Isotopic Ratios								Ages (Ma)			
Fraction	U (ppm)	Pb (ppm)	Pb_c (pg)	$^{206}Pb^*/^{204}Pb$	$^{207}Pb/^{235}U$	± (%)	$^{206}Pb/^{238}U$	± (%)	Corr. Coef	$^{207}Pb/^{206}Pb^*$	± (%)	$^{207}Pb/^{235}U$	±	$^{206}Pb/^{238}U$	±	$^{207}Pb/^{206}Pb$	±	Conc. distance (%)
Z1 (L8)	169.9	63.8	6.1	1656.98	5.66072	0.45	0.34069	0.31	0.69	0.12051	0.33	1925.4	3.9	1890.0	5.1	1963.7	5.9	+1.8
Z2 (L9)	412.3	193.2	16.4	214.00	5.70500	0.47	0.34257	0.34	0.76	0.12078	0.30	1932.1	4.0	1899.0	5.7	1967.8	5.4	+1.7
Z3 (L10)	274.2	111.0	13.5	404.38	5.52579	0.43	0.33293	0.36	0.85	0.12038	0.23	1904.6	3.7	1852.6	5.8	1961.8	4.1	+3.2

Z: zircon, L: minibomb number (lab code).
All fractions were chemically abraded (CA technique; Mattison (2005).

Table 4. Zircon U-Pb CA-ID-TIMS isotopic data for sample E33D009I (rhyolite).

Tabla 4. Datos isotópicos U-Pb CA-ID-TIMS en circón para la muestra E33DR001I (riolita).

4. Discussion and conclusions

Our new U-Pb zircon geochronology data for plutonic and volcanic rocks of the Menongue Igneous Complex, with crystallization ages ranging from 1982.4 ± 22.9 Ma to 1949.3 ± 10.2 Ma, clearly demonstrate that the magmatic activity responsible for its emplacement within the Cassinga Zone occurred during the Eburnean Event. The overlapping crystallization ages of the monzogranite (1968.8 ± 6.2 Ma) and rhyolite (1963.9 ± 2.8 Ma) strongly support field evidence suggesting contemporaneous emplacement of the volcanic and plutonic facies (Lopes *et al*., 2021). Furthermore, our data indicate that the magmatism of the Menongue Igneous Complex is coeval with granitoids and felsic volcanic rocks from Conda, in the northwestern part of the Central Eburnean Zone, dated between 1978 ± 11 Ma and 1964 ± 9 Ma (Delor *et al*., 2006, in Jelsma *et al*., 2018). However, our findings refute previously proposed correlations (e.g., BRGM, 1970b, c; Pascal, 2006; Pereira *et al*., 2013) with the Matala felsic subvolcanic rocks of the Cassinga Zone, dated at 1440 ± 6 Ma (Merino-Martínez *et al*., under review), as well as with those from Chibia–Cainde in the southern part of the Central Eburnean Zone, dated at 1814 ± 8 Ma and 1804 ± 7 Ma (Pereira *et al*., 2013).

Eburnean-aged granitoids and their metamorphic equivalents constitute a significant portion of the Angolan basement within the Angolan Shield (Fig. 1), being largely predominant in the Central Eburnean Zone (2038 ± 28 to 1947 ± 5 Ma; Pereira *et al*., 2011; McCourt *et al*., 2013; Milani *et al*., 2022; Merino-Martínez *et al*., under review) and intruding into the Neoarchean crust of the Central Shield Zone (1973.5 ± 4.9 Ma to 1965.6 ± 3.1 Ma; Jelsma *et al*., 2018). In northern Namibia, south and southeast of the late Orosirian to early Statherian Epupa Metamorphic Complex, several Paleoproterozoic inliers comprising Eburnean granitoids and gneisses are exposed (Fig. 1). These Eburnean granitoids, dated between 2028 ± 15 Ma and 1933.4 ± 3.1 Ma (Seth *et al*., 1998; Franz *et al*., 1999; Kröner *et al*., 2004; Kröner, 2005; Luft *et al*., 2011), intrude into 2645 ± 6 to 2584 ± 1 Ma granitoid-gneisses in the Sesfontein Inlier (Seth, 1999). Further east, granitoids and granitoid-gneisses dated between 2050.5 ± 0.6 Ma and 1937 ± 27.3 Ma have also been reported in the Kamanjab, Grootfontein, Tsumkwe, and Quangwadum inliers. (Fig. 1; Hoal *et al*., 2000; Sanz, 2005; Singletary *et al*., 2003) (Table 5). The prevalence of crustal reworking in the generation of Eburnean magmas is evident from the abundance of zircon xenocrysts and/or inherited cores (ca. 2.83, 2.82, 2.62, 2.60, 2.54–2.47, 2.29, 2.26, and 1.99 Ga), notably negative $\varepsilon Nd_{(i)}$ (-3.0 to -8.0) and $\varepsilon Hf_{(i)}$ (-6.9 to -11.7) values, and Meso- to Neoarchean Nd (3.14 to 2.67 Ga) and Hf (3.08 to 2.89 Ga) TDM_2 ages in Eburnean granitoids and orthogneisses across the Angolan Shield (Table 5). Crustal reworking is further supported by similarly markedly negative $\varepsilon Hf_{(i)}$ values (average = -8.5 ± 4.4) and Meso- to Neoarchean TDM_2 ages (average = 2.94 ± 0.20 Ga) of Eburnean zircons preserved in the tabular Mesoproterozoic siliciclastic sequences from the Namibe Zone (Ferreira *et al*., 2024). The presence of an inherited core dated at 2672 ± 66 Ma and xenocrysts dated at 2091 ± 20 Ma and 2048 ± 24 Ma in the syenogranite and dacite of the Menongue area strongly suggests that crustal reworking and assimilation were also important factors in the generation of the Menongue Igneous Complex magmas.

The Paleoproterozoic magmatism in the Angolan Shield has traditionally been interpreted as the product of a long-lived Andean-type continental arc (~2000 ± 200 Ma) along the southwestern margin of the Congo Craton (Seth, 1999; Kleinhanns *et al*., 2013; McCourt *et al*., 2013; Jelsma *et al*., 2018; Kröner *et al.,* 2015). However, recent PLANAGEO geological mapping and Hf-Nd isotopic compositions have led to a reinterpretation of the Eburnean magmatism (ca. 2050 to 1933 Ma) in the Angolan Shield as a product of a collisional orogeny related to the amalgamation of independent Archean crustal blocks during the assembly of the supercontinent Columbia (Merino-Martínez *et al*., 2021; Rodrigues *et al*., 2021; Ferreira *et al*., 2024). The geotectonic significance of the Menongue Igneous Complex and the Cassinga Zone within the context of Columbia assembly remains to be established. Future detailed whole-rock geochemistry and zircon U-Pb and Lu-Hf studies of the Eburnean record in the Cassinga Zone shall provide valuable insights into this topic.

Location	Lithology	Lat	Long	Crystallization ages (Ma)		Inherited cores/ Xenocrysts (Ma)		$\varepsilon Nd_{(i)}$	$Hf_{(i)}$	TDM_2 (Ga)	Source
Central Shield Zone	Gneissic bt-granite	-12.532	16.699	1973.5	4.9	2599	7				Jelsma et al., 2018
	Massive quartz diorite	-11.420	17.013	1972.7	6.9	2515	14				
						2816	8				
	Megacrystic biotite gneiss	-11.614	16.652	1972	4.4	2539	14				
						2617	24				
						2832	12				
	Granodiorite	-11.389	16.275	1967.5	4.5						
	Granodioritic augen gneiss	-11.389	16.275	1965.6	3.1						
Central Eburnean Zone	Bt-granite	-14.71806	13.46778	1947	5			-5.1		2.82	Pereira et al., 2011
	Porphyritic granite	-15.05017	13.23967	2038	28	2263	12				McCourt et al.. 2013
	Equigranular granite	-14.84217	13.43917	1953.8	6.4						
	Granite	-14.80007	14.42531	1964	3	1992.2	9.6		-6.9 to -9.7	2.87 to 2.97	Milani et al.. 2022
	Granodiorite	-15.83745	13.9355	1947	4	2467	10		-9.8 to -11.7	2.98 to 3.08	
	Foliated porphyritic granite	-14.44508	12.83139	1989	12						Merino-Martínez et al., under review.
	Foliated granite	-14.21536	12.87905	1987	7						
	Bt-granite-gneiss	-15.34228	13.57773	1987.1	7.3						
	Schlieric monzogranite	-14.26884	13.79871	1984	19						
	Granite gneiss	-14.88324	14.44266	1981	6						
	Granite	-16.1382	15.86794	1975	10						
	Granite gneiss	-14.4351	15.06929	1971	11						

Cassinga Zone	Granite	-15.67848	15.76044	1981.8	7.5					Merino-Martínez et al., under review.
	Syenogranite	-14.499	17.765	1982.4	22.9	2672	66			
	Bt-hbl-monzogranite	-14.859	17.169	1968.8	6.2					
	Porphyritic rhyolite	-16.181	15.759	1963.9	2.8					This study
	Porphyritic dacite	-14.328	17.488	1949.3	10.2	2048	24			
						2091	20			
Sesfontein Inlier	Diorite-gneiss	-19.22675	13.39063	1985	23	2287	10	-6.7	2.97	
						2605	11			
	Diorite-gneiss	-19.295	13.34817	1974.4	1.2			-6.7	2.97	
	Granitic gneiss	-19.28633	13.31383	1971	7			-8.9	3.14	Seth, 1999
	Alkali granitic augengneiss	-18.94233	13.46333	1964.7	1.3			-5.7	2.88	
	Partly migmatised diorite-gneiss	-19.21127	13.37143	1963.6	7.2			-6.7	2.96	
	Granodioritic augengneiss	-19.19633	13.435	1961	4			-5.6	2.87	
	Orthogneiss	13.313909	-19.2826	1933.4	3.1					Franz et al., 1999
	Granite-gneiss	-18.8962	13.1102	2028	15					Kroner, 2005
	Migmatitic granodiorite-gneiss	-18.8515	12.8764	2008	18			-4.0	2.79	
	Granodiorite-gneiss	-18.726	12.985	1979	38			-3.5	2.72	
	Granodiorite augen-gneiss	-19.295	13.284	1971	9.3			-3.0	2.67	Luft et al., 2011
Kamanjab Inlier	Alk-granite	14.392412	-19.3156	1937.3	36.2	2500	38			Sanz, 2005
	Qtz-monzonite	14.387133	-19.4422	1937	27.3					
Grootfontein Inlier	Granite-gneiss	-19.643	20.818	2022	15					Hoal et al., 2000
Quangwadum Complex	Augengneiss	-19.539	21.196	2050.5	0.6			-3.8	2.80	Singletary et al., 2003

Table 5. U-Pb zircon crystallization and inherited/xenocrystic ages, along with Nd (whole-rock) and Hf (zircon) isotopic data, for Eburnean rocks from the different geotectonic zones of the Angolan Shield.

Tabla 5. Edades U-Pb de cristalización y de núcleos heredados o xenocristales (circón), así como datos isotópicos de Nd (roca total) y Hf (circón) para rocas Eburneanas de las diferentes zonas geotectónicas del Escudo de Angola.

5. Acknowledgements

This research was conducted as part of the National Geological Plan of Angola (PLANAGEO). PLANAGEO was sponsored by the Government of the Republic of Angola and executed by the Geological Survey of Angola (IGEO), under the supervision of the Angolan Ministry of Mineral Resources, Oil, and Gas (MIREMPET). We gratefully acknowledge the invaluable logistical support provided by Impulso Industrial Alternativo during PLANAGEO. We also thank João Lains Amaral and Luis Albardeiro for their constructive comments and suggestions, which improved the manuscript.

Authorship contribution statement

Ezequiel Ferreira: Writing - Original Draft, Writing - Review & Editing, Conceptualization, Formal Analysis, Visualization.
Pablo Valverde-Vaquero: Investigation, Formal Analysis, Visualization.
Miguel Gutíerrez-Medina: Writing - Review & Editing, Resources.
Jorge Buzzi-Marcos: Writing - Review & Editing, Resources.
Rui Lopes: Writing - Review & Editing, Resources.
Juan Carlos Gumiel: Resources.
Enrique Merino-Martínez: Conceptualization, Supervision.
Aratz Beranoaguirre: Investigation.
María del Carmen Feria: Visualization.
Pilar Montero: Investigation, Validation.
José Manuel: Funding acquisition, Project administration.

6. References

Bassot, J.P., Pascal, M., & Vialette, Y. (1980/1981). Données nouvelles sur la stratigraphie, la géochimie et la géochronologie des formations précambriennes de la partie méridionale du Haut Plateau angolais. Bulletin du B.R.G.M. (deuxième série). Section IV. n°4-1980/1981, 285-309.

Black, L., Kamo, S., Allen, C., Aleinikoff, J., Davis, D., Korsch, R., & Foudoulis, C. (2003). TEMORA 1: a new zircon standard for Phanerozoic U–Pb geochronology. Chemical Geology, 200, 155-170. https://doi.org/10.1016/S0009-2541(03)00165-7

BRGM (1970a). Rapport de fin de Mission. Cartographie a 1/250 000 des concessions C.M.L. (Angola). Notice explicative feuille SD 33 X Cassinga. 73 RME 014 AF, 1-13.

BRGM (1970b). Rapport de fin de Mission. Cartographie a 1/250 000 des concessions C.M.L. (Angola). Notice explicative feuille SD 33 Z Chitanda. 73 RME 014 AF, 1-9.

BRGM (1970c). Rapport de fin de Mission. Cartographie a 1/250 000 des concessions C.M.L. (Angola). Notice explicative feuille SD 33 Z Serpa Pinto. 73 RME 014 AF, 1-11.

Buzzi, J., & Gutiérrez-Medina, M. (2022). Carta Geológica de Angola à escala 1:250.000, folha Sul D-33/X (Cassinga) e memória explicativa. UTE (IGME-LNEG-Impulso) – IGEO, Luanda, Angola.

Bybee, G.M., Hayes, B., Owen-Smith, T.M., Lehmann, J., Ashwal, L.D., Brower, A.M., Hill, C.M., Corfu, F., & Manga, M. (2019). Proterozoic massif-type anorthosites as the archetypes of long-lived (≥100 Myr) magmatic systems – New evidence from the Kunene Anorthosite Complex (Angola). Precambrian Research, 332, 105393. https://doi.org/10.1016/j.precamres.2019.105393

Carvalho, H. (1981). Geologia de Angola, folhas n° 1-4, escala 1:1.000.000. Laboratório Nacional de Investigação Científica Tropical.

Carvalho, H. (1984). Estratigrafia do Precâmbrico de Angola. Garcia de Orta, Série de Geologia, 7, 1-66.

Carvalho, H., & Alves, P. (1993). The Precambrian of SW Angola and NW Namibia. General Remarks. Correlation Analysis. Economic Geology. Comunicações do Instituto de Investigação Científica Tropical, 4, 1-38.

Carvalho, H., Tassinari, C., Alves, P.H., Guimarães, F., & Simões, M.C. (2000). Geochronological review of the Precambrian in western Angola: links with Brazil. Journal of African Earth Sciences, 31, 383-402. https://doi.org/https://doi.org/10.1016/S0899-5362(00)00095-6

Claoué-Long, J.C., Compston, W., Roberts, J., & Fanning, C.M. (1995). Two Carboniferous ages: a comparison of SHRIMP zircon dating with conventional zircon ages and $^{40}Ar/^{39}Ar$ analysis. In: Berggren, W.A., Kent, D.V., Aubry, M.-P., & Hardenbol, J. (Eds.), Geochronology, Time Scales and Global Stratigraphic Correlation. SEPM Special Publication 54, Society for Sedimentary Geology, Tulsa, Oklahoma, USA, 3-21. https://doi.org/10.2110/pec.95.04.0003

Ferreira, E., Lehmann, J., Feliciano Rodrigues, J., Hayes, B., Merino-Martínez, E., Milani, L., Bybee, G., Owen Smith, T., Luis García-Lobón, J., C. G. Tassinari, C., Ueckermann, H., Sato, K., Bravo Silva, P., Correia, J., Labaredas, J., Duarte, L., Molekwa, M.A., Manuel, J., & Victorino, A.M.L. (2024). Zircon U-Pb and Lu-Hf isotopes reveal the crustal evolution of the SW Angolan Shield (Congo Craton). Gondwana Research, 131, 317-342. https://doi.org/10.1016/j.gr.2024.03.010

Franz, L., Romer, R., & Dingeldey, D. (1999). Diachronous Pan-African granulite-facies metamorphism (650 Ma and 550 Ma) in the Kaoko Belt, NW Namibia. European Journal of Mineralogy, 11, 167-180.

Goscombe, B., Foster, D.A., Gray, D., Wade, B., Marsellos, A., & Titus, J. (2017). Deformation correlations, stress field switches and evolution of an orogenic intersection: The Pan-African Kaoko-Damara orogenic junction, Namibia. Geoscience Frontiers, 8, 1187-1232. https://doi.org/10.1016/j.gsf.2017.05.001

Gumiel, J., Martín-Banda, R., Iglesias-Martínez, M., & Goicoechea, P. (2021). Carta Geológica de Angola à escala 1:250.000, folha Sul E-33/D e Sul E-33/J (Ondjiva) e memória explicativa. UTE (IGME-LNEG-Impulso) – IGEO, Luanda, Angola.

Gutiérrez-Medina, M., & Buzzi, J. (2021). Carta Geológica de Angola à escala 1:250.000, folha Sul D-33/R (Menongue) e memória explicativa. UTE (IGME-LNEG-Impulso) – IGEO, Luanda, Angola.

Hoal, K., Hoal, B., Griffin, W., & Armstrong, R. (2000). Characterization of the age and nature of the lithosphere in the Tsumkwe region Namibia. Communications, Geological Survey of Namibia, 12, 23-30.

Isachen, C., Coleman, D., & Schmitz, M. (2007). Pb MacDat program. http://www.earthtime.org. Last accessed in 2015.

Jelsma, H., McCourt, S., Perritt, S., & Armstrong, R. (2018). The Geology and Evolution of the Angolan Shield, Congo Craton. In: Siegesmund, S., Basei, M., Pedro, O., & Oriolo, S. (Eds.), Geology of Southwest Gondwana. 217-239. https://doi.org/10.1007/978-3-319-68920-3_9

Kleinhanns, I.C., Fullgraf, T., Wilsky, F., Nolte, N., Fliegel, D., Klemd, R., & Hansen, B.T. (2013). U–Pb zircon ages and (isotope) geochemical signatures of the Kamanjab Inlier (NW Namibia): constraints on Palaeoproterozoic crustal evolution along the southern Congo craton. Geological Society London Special Publications, 389, 165-195. https://doi.org/10.1144/SP389.1

Kopershoek, H.R. (1984). The geology of the Cassinga district Angola and its potencial as compared to that of Serra dos Carajás, Brazil. 33° Congresso Brasileiro de Geologia. Sociedade Brasileira de Geologia, Rio de Janeiro.

Kopershoek, H.R. (1970). Geology of the Cassinga north area; explanatory note of the 1/50.000 geological map. Rel. Comp. Min. Lobito, Jamba (inédito).

Krogh, T.E. (1973). A low-contamination method for hydrothermal decomposition of zircon and extraction of U and Pb for isotopic age determinations. Geochimica et Cosmochim Acta, 37, 485-494. https://doi.org/10.1016/0016-7037(73)90213-5

Kröner, S., Konopásek, J., Kröner, A., Passchier, C., Poller, U., Wingate, M., & Hofmann, K. (2004). U-Pb and Pb-Pb zircon ages for metamorphic rocks in the Kaoko Belt of Northwestern Namibia: A Palaeo- to Mesoproterozoic basement reworked during the Pan-African orogeny. South African Journal of Geology, 107, 455-476.

Kröner, S. (2005). Geochronological and Structural Evolution of the Western and Central Kaoko Belt in NW Namibia. PhD thesis, Johannes Gutenberg-Universität Mainz, Mainz. https://doi.org/10.25358/openscience-1899

Kröner, A., Rojas-Agramonte, Y., Hegner, E., Hoffmann, K.H., & Wingate, M.T.D. (2010). SHRIMP zircon dating and Nd isotopic systematics of Palaeoproterozoic migmatitic orthogneisses in the Epupa Metamorphic Complex of northwestern Namibia. Precambrian Research, 183, 50-69. https://doi.org/10.1016/j.precamres.2010.06.018

Kröner, A., Rojas-Agramonte, Y., Wong, J., & Wilde, S.A. (2015). Zircon reconnaissance dating of Proterozoic gneisses along the Kunene River of northwestern Namibia. Tectonophysics, 662, 125-139. https://doi.org/10.1016/j.tecto.2015.04.020

Lehmann, J., Bybee, G.M., Hayes, B., Owen-Smith, T.M., & Belyanin, G. (2020). Emplacement of the giant Kunene AMCG complex into a contractional ductile shear zone and implications for the Mesoproterozoic tectonic evolution of SW Angola. International Journal of Earth Sciences, 109, 1463-1485. https://doi.org/10.1007/s00531-020-01837-5

Lopes, R., Máximo, J., & Sousa, J.C. (2021). Carta Geológica de Angola à escala 1:250.000, folha Sul D-33/Z (Caiundo) e memória explicativa (2a edição). UTE (IGME-LNEG-Impulso) – IGEO, Luanda, Angola.

Luft, J.L., Chemale, F., & Armstrong, R. (2011). Evidence of 1.7- to 1.8-Ga collisional arc in the Kaoko Belt, NW Namibia. International Journal of Earth Sciences, 100, 305-321. https://doi.org/10.1007/s00531-010-0591-5

Mattinson, J.M. (2005). Zircon U–Pb chemical abrasion (“CA-TIMS”) method: Combined annealing and multi-step partial dissolution analysis for improved precision and accuracy of zircon ages. Chemical Geology, 220, 47-66. https://doi.org/10.1016/j.chemgeo.2005.03.011

McCourt, S., Armstrong, R.A., Jelsma, H., & Mapeo, R.B.M. (2013). New U-Pb SHRIMP ages from the Lubango region, SW Angola: Insights into the Palaeoproterozoic evolution of the Angolan Shield, southern Congo Craton, Africa. Journal of the Geological Society of London, 170, 353-363. https://doi.org/10.1144/jgs2012-059

Merino-Martínez, E., Rodrigues, J.F., & Ferreira, E. (2021). Mapa Geológico de Angola à escala 1:1.000.000 e Notícia Explicativa. UTE (IGME-LNEG-Impulso) – IGEO, Luanda, Angola.

Merino-Martínez, E., Ferreira, E., Valverde-Vaquero, P., Rodrigues, J.F., Escuder-Viruete, J., García-Lobón, J.L., Beranoaguirre, A., Feria, M.C., Rey-Moral, C., Bravo Silva, P., González-Cuadra. P., Sousa, J.C., Potti, J., Máximo, J., Gutiérrez-Medina, M., Gumiel, J.C., Galan, G., Mochales, T., Manuel, J., Cordeiro, D., Tassinari, C., Montero, P., Sato, K., Montero, P., Fuenlabrada, J.M., & Galindo, C. (under review). Pre-Mesoproterozoic crustal framework and Mesoproterozoic evolution of the SW Angolan Shield: structural, geochemical, and isotopic insights from the Kunene Complex and surrounding basement. Precambrian Research .

Milani, L., Lehmann, J., Bybee, G.M., Owen-Smith, T.M., Oosthuizen, L., Delport, P., & Ueckermann, H. (2022). Geochemical and geochronological constraints on the Mesoproterozoic Red Granite Suite, Kunene AMCG Complex of Angola and Namibia. Precambrian Research, 379, 106821. https://doi.org/10.1016/j.precamres.2022.106821

Mouta, F. (1933). Descrição da Carta Geológica de Angola. Lisboa. Agência Geral das Colónias. Divisão de Publicações e Biblioteca. Colecção de Relatórios, Estudos e Documentos Coloniais, 38 p.

Mouta, F. (1954). Notícia Explicativa do Esboço Geológico de Angola (1:2.000.000). Lisboa. Ministério do Ultramar, Junta de Investigações do Ultramar, 148 p.

Pascal, M. (1980). Etude géologique des formations précambriennes du haut-plateau méridional de l’Angola. Université Scientique et Médicale de Grenoble, Grenoble.

Pascal, M. (2006). Carta Geológica do Planalto Meridional de Angola, 1:500.000. BRGM – IGEO, República de Angola.

Pereira, E., Tassinari, C.C.G., Rodrigues, J.F., & Van-Dúnem, M.V. (2011). New data on the deposition age of the volcano-sedimentary Chela Group and its Eburnean basement: implications to post-Eburnean crustal evolution of the SW of Angola. Comunicações Geológicas, 98, 29-40.

Pereira, E., Rodrigues, J.F., Tassinari, C.C.G., & Van-Dúnen, M.V. (2013). Geologia da região de Lubango, SW de Angola: evolução no contexto do cratão do Congo. LNEG – IGEO, Luanda, Angola.

Pereira, E., Ferreira, E., Rodrigues, J., & Merino Martínez, E. (2021). Mapa Geológico de Angola, escala 1:500.000, Bloco UTE-2, e notícia explicativa. Luanda, Angola.

Rodrigues, J.F., Merino Martínez, E., Ferreira, E., and Francés, A. (2021). Mapa Tectónico de Angola à escala 1:1.000.000 e notícia explicativa. UTE (IGME-LNEG-Impulso) – IGEO, Luanda, Angola.

Sanz, A.L.G. (2005). Pre- and Post-Katangan Granitoids of the Greater Lufilian Arc - Geology, Geochemistry, Geochronology and Metallogenic Significance. PhD thesis. University of the Witwatersrand, Johannesburg.

Seth, B. (1999). Crustal evolution of the Kaoko belt, NW Namibia. Geochemical and geochronological study of Archaean to Mesoproterozoic basement gneisses and Pan-African migmatites and granitoids. Julius Maximilian University of Würzburg, Würzburg, Germany.

Seth, B., Kröner, A., Mezger, K., Nemchin, A.A., Pidgeon, R.T., & Okrusch, M. (1998). Archaean to Neoproterozoic magmatic events in the Kaoko belt of NW Namibia and their geodynamic significance. Precambrian Research, 92, 341-363. https://doi.org/10.1016/S0301-9268(98)00086-2

Silva, A. (2005). A geologia da República de Angola desde o Paleoarcaico ao Paleozóico Inferior.

Singletary, S., Hanson, R., Martin, M., Crowley, J., Bowring, S., Key, R., Ramokate, L., Direng, B., & Krol, M. (2003). Geochronology of basement rocks in the Kalahari Desert, Botswana, and implications for regional Proterozoic tectonics. Precambrian Research, 121, 47-71. https://doi.org/10.1016/S0301-9268(02)00201-2

Söderlund, U., & Johansson, L. (2002). A simple way to extract baddeleyite (ZrO_2). Geochemistry, Geophysics, Geosystems, 3. https://doi.org/10.1029/2001GC000212

Sousa, J.C., Oliveira, A., & Máximo, J. (2021a). Carta Geológica de Angola à escala 1:250.000, folha Sul D-33/Q (Jamba) e memória explicativa (2a edição). UTE (IGME-LNEG-Impulso) – IGEO, Luanda, Angola.

Sousa, J.C., Oliveira, A., & Máximo, J. (2021b). Carta Geológica de Angola à escala 1:250.000, folha Sul D-33/V (Cuvelai) e memória explicativa (2a edição). UTE (IGME-LNEG-Impulso) – IGEO, Luanda, Angola.

Stacey, J.S., & Kramers, J.D. (1975). Approximation of terrestrial lead isotope evolution by a two-stage model. Earth and Planetary Science Letters, 26, 207-221. https://doi.org/10.1016/0012-821X(75)90088-6.

Valverde-Vaquero, P. (2009). Método de datación U-Pb ID-TIMS en el laboratorio geocronológico del IGME (Tres Cantos). VII Congreso Ibérico, X Congreso Nacional de Geoquímica, Soria.

Vermeesch, P. (2018). IsoplotR: a free and open toolbox for geochronology. Geoscience Frontiers, 9, 1479-1493, doi: https://doi.org/10.1016/j.gsf.2018.04.001

Williams, I.S., & Claesson, S. (1987). Isotopic evidence for the Precambrian provenance and Caledonian metamorphism of high grade paragneisses from the Seve Nappes, Scandinavian Caledonides. Contributions to Mineralogy and Petrology, 97, 205-217. https://doi.org/10.1007/BF00371240